



# Soil moisture balance and magnetic enhancement in loess–paleosol sequences from the Tibetan Plateau and Chinese Loess Plateau



Pengxiang Hu<sup>a,b</sup>, Qingsong Liu<sup>a,\*</sup>, David Heslop<sup>c</sup>, Andrew P. Roberts<sup>c</sup>, Chunsheng Jin<sup>a</sup>

<sup>a</sup> Division of Tethys Research Center, Institute of Geology and Geophysics, Chinese Academy of Sciences, Beijing 100029, People's Republic of China

<sup>b</sup> University of the Chinese Academy of Sciences, Beijing 100049, People's Republic of China

<sup>c</sup> Research School of Earth Sciences, The Australian National University, Canberra, ACT 0200, Australia

## ARTICLE INFO

### Article history:

Received 5 May 2014

Received in revised form 3 October 2014

Accepted 19 October 2014

Available online xxxxx

Editor: J. Lynch-Stieglitz

### Keywords:

Chuanxi loess  
environmental magnetism  
loess provenance  
pedogenesis  
climate  
soil moisture

## ABSTRACT

We present a first combined environmental magnetic and geochemical investigation of a loess–paleosol sequence (<55 ka) from the Chuanxi Plateau on the eastern margin of the Tibetan Plateau. Detailed comparison between the Ganzi section and the Luochuan section from the Chinese Loess Plateau (CLP) allows quantification of the effects of provenance and climate on pedogenic magnetic enhancement in Chinese loess. Rare earth element patterns and clay mineral compositions indicate that the Ganzi loess originates from the interior of the Tibetan Plateau. The different Ganzi and CLP loess provenances add complexity to interpretation of magnetic parameters in terms of the concentration and grain size of eolian magnetic minerals. Enhanced paleosol magnetism via pedogenic formation of ferrimagnetic nanoparticles is observed in both sections, but weaker ferrimagnetic contributions, finer superparamagnetic (SP) particles and stronger chemical weathering are found in the Ganzi loess, which indicates the action of multiple pedogenic processes that are dominated by the combined effects of mean annual precipitation (MAP), potential evapotranspiration (PET), organic matter and aluminium content. Under relatively high MAP and low PET conditions, high soil moisture favours transformation of ferrimagnetic minerals to hematite, which results in a relatively higher concentration of hematite but weaker ferrimagnetism of Ganzi loess. Initial growth of superparamagnetic (SP) particles is also documented in the incipient loess at Ganzi, which directly reflects the dynamic formation of nano-sized pedogenic ferrimagnets. A humid pedogenic environment with more organic matter and higher Al content also helps to form finer SP particles. We therefore propose that soil water balance, rather than solely rainfall, dominates the type, concentration and grain size of secondary ferrimagnetic minerals produced by pedogenesis.

© 2014 Elsevier B.V. All rights reserved.

## 1. Introduction

Environmental magnetism is an interdisciplinary subject that involves a wide spectrum of geological and environmental problems (Dekkers, 1997; Q.S. Liu et al., 2012 and references therein; Oldfield, 1991; Thompson and Oldfield, 1986; Verosub and Roberts, 1995). Loess deposits provide semi-continuous records of terrestrial paleoclimate and are a key archive with which to reconstruct monsoon evolution, aridification history, and abrupt climate change using magnetic properties (An, 2000; Deng et al., 2006; Ji et al., 2004; Liu et al., 2007 and references therein). However, loess magnetism depends on different regional paleoenvironmental factors, which complicates magnetic interpretation. For instance,

the magnetism of loess–paleosol sequences in Alaska and Siberia is explained by a wind-vigour model, whereby eolian iron oxide grains play a dominant role in controlling magnetic properties (Begét et al., 1990; Chlachula et al., 1998). In contrast, loess sequences in Eastern Asia and Europe contain magnetically enhanced paleosol layers that result from pedogenic formation of ultrafine superparamagnetic (SP) and single domain (SD) magnetite and/or maghemite grains (Boyle et al., 2010; Dearing et al., 1996; Liu et al., 2007; Zhou et al., 1990). Therefore, to understand the environmental magnetic signal carried by loess–paleosol sequences, two key problems must be addressed. First, magnetic minerals from different sources must be identified, characterized and quantified. Second, the identified minerals must be attributed to specific environmental processes.

Many studies have addressed the first problem through use of rock magnetic and mineralogical methods (Egli, 2004; Geiss and Zanner, 2006; Heslop et al., 2002; Heslop and Roberts, 2012a; Roberts et al., 2000, 2006). Hu et al. (2013) integrated dynamic

\* Corresponding author at: Division of Tethys Research Center, Institute of Geology and Geophysics, Chinese Academy of Sciences, Beijing 100029, People's Republic of China. Tel.: +86 10 82998365; fax: +86 10 62010846.

E-mail address: liux0272@yahoo.com (Q. Liu).

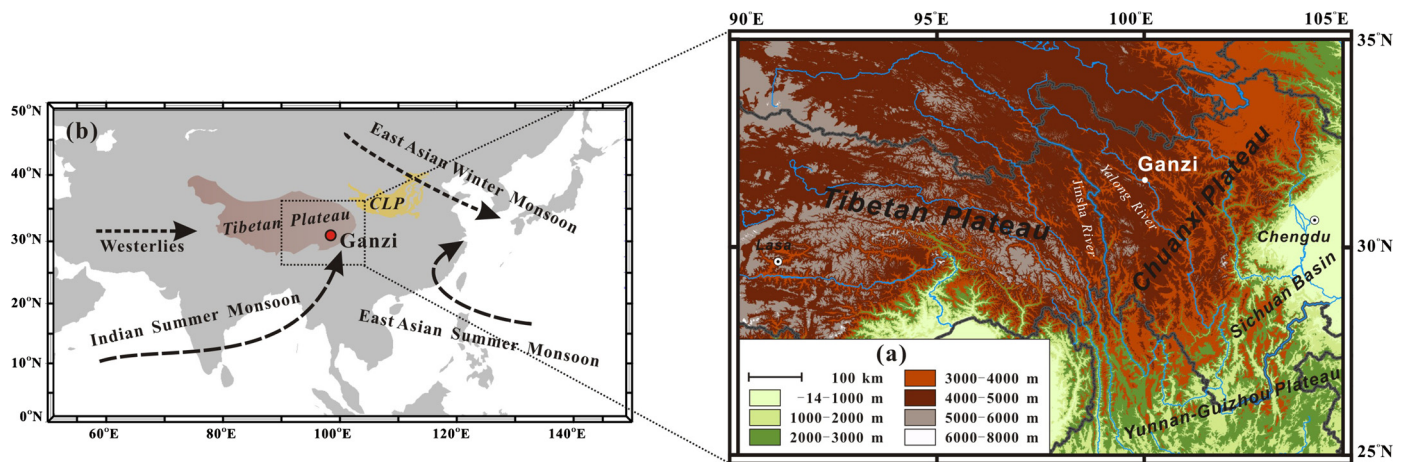


**Fig. 1.** (a) Map with regional elevations and location of the Ganzi section and adjacent areas. Elevation data are from the International Scientific & Technical Data Mirror Site, Computer Network Information Center, Chinese Academy of Sciences. (b) Schematic map of the studied area with monsoon illustration. The Ganzi area is mainly under the influence of the Indian monsoon flow from the Arabian Sea and Bay of Bengal in summer and westerlies during winter. In contrast, the East Asian Summer and Winter monsoon is the dominant atmospheric circulation system on the CLP.

dissolution, rock magnetic and diffuse reflectance spectrometer (DRS) techniques to separate and quantify lithogenic and pedogenic magnetic minerals in Chinese loess. The aim of this paper is to build on previous work to evaluate environmental factors that control the magnetic properties of loess–paleosol sequences. The influence of provenance factors on soil magnetism, such as Fe supply (Dearing et al., 1996; Maher, 1998), topography (Liu and Liu, 2014), and climatic factors, such as mean annual precipitation (MAP) and potential evapotranspiration (PET) (Balsam et al., 2011; Liu et al., 2013; Maher et al., 1994; Orgeira et al., 2011; Porter et al., 2001) have been investigated in modern soils. In well-studied parts of the Chinese Loess Plateau (CLP) loess–paleosol sequences (e.g. the Malan loess), which are developed on similar topography, provenance and climate have been shown to be the most important factors that control the magnetic signal (Evans and Heller, 2001; Liu et al., 2007). On this basis, comparative environmental magnetic studies on loess–paleosol sequences in different climate zones with different source areas are needed urgently.

Loess–paleosol sequences are widely distributed in China, which provides an opportunity for comparative studies. Environmental magnetic investigations have been performed widely on loess deposits from the CLP, but comparative studies outside the CLP are rare despite their potential to provide insights into relationships between magnetic properties, climate and source material variations (Y. Liu et al., 2012; Wei et al., 2013; Zan et al., 2010; Zhang et al., 2007). Continuous loess deposition also occurred over the Chuanxi Plateau, southeastern Tibetan Plateau (Fig. 1a). The climate of the Chuanxi Plateau is largely controlled by interactions among the Tibetan monsoon, Indian monsoon and westerlies (Chen et al., 2002; Pan and Wang, 1999), and the loess source area is potentially different from the CLP (Fang, 1994; Fang et al., 1996; Qiao et al., 2006; Wang et al., 2003). Therefore, the Chuanxi loess provides an opportunity to quantify the effects of source material and climate on pedogenic magnetic mineral formation. We present an integrated rock magnetic, geochemical and DRS investigation of a Chuanxi loess–paleosol sequence, which has been forming since ~55 ka. By comparing the Chuanxi loess–paleosols to contemporaneous CLP deposits, we provide new lines of evidence concerning the dominant factors that influence the magnetism of loess–paleosol sequences.

## 2. Material and methods

### 2.1. Geographic setting and sampling

The Chuanxi Plateau is bordered by the Sichuan Basin to the east, the Jinsha River to the west and the Yunnan–Guizhou Plateaus to the south. Its elevation decreases from 4000–4500 m in the west to 3000–3500 m in the east (Fig. 1a). As a result of multiple Quaternary uplift episodes of the Tibetan Plateau, river terraces have formed by erosion. Loess deposits are widely and continuously distributed over higher river terraces. The Ganzi loess section (31°30.994'N, 99°58.590'E, 3455 m elevation) is located in the western Chuanxi Plateau (Fig. 1a). MAP in this area is 660 mm (30 yr average from 1971 to 2000). Most precipitation occurs in the summer (May to September), which accounts for ~81% of the annual total. The mean annual temperature (30 yr average from 1971 to 2000) is 5.6 °C, with a maximum of 13.9 °C in July and a minimum of –4.4 °C in January. Today, the Ganzi section is under the influence of the Indian monsoon and westerlies in summer and winter, respectively (Fig. 1b).

The Ganzi section is located on the fifth terrace of the Yalong River (Fig. 1a). It has a thickness of 14.5 m and is composed of seven main units, which are described following the CLP convention: (1) a brown cultivated topsoil, which is excluded from this study; (2) modern loess – L0; (3) a Holocene paleosol – S0; (4) the last glacial Malan loess – L1, which in turn includes two loess sub-layers (L1L1 and L1L2) and two weakly developed paleosols (L1S1 and L1S2). These layers are described in Table A.1. The section was sampled at 2-cm stratigraphic intervals for this study; 725 samples were collected. Five samples for optically stimulated luminescence (OSL) dating were taken by driving stainless steel tubes into the fresh outcrop at each stratigraphic boundary. Fine quartz particles were selected for OSL dating and were prepared following J.F. Liu et al. (2010). Measurements were performed using a Daybreak 1100 TL/OSL automatic measurement system in the Luminescence Dating Laboratory of the State Key Laboratory of Earthquake Dynamics, Institute of Geology, China Earthquake Administration. The five resulting OSL ages are shown in Fig. 2a, which demonstrate that the Ganzi section has been forming since the early part of marine isotope stage (MIS) 3 (dated at  $55.2 \pm 2.7$  ka).

We compare the Ganzi loess that was deposited through the last glacial cycle (including S0, L1L1, L1S1, L1L2, L1S2) to contemporaneous material from the Luochuan section on the central CLP (Fig. 3). MAP at Luochuan is 511 mm (1971 to 2000), with summer

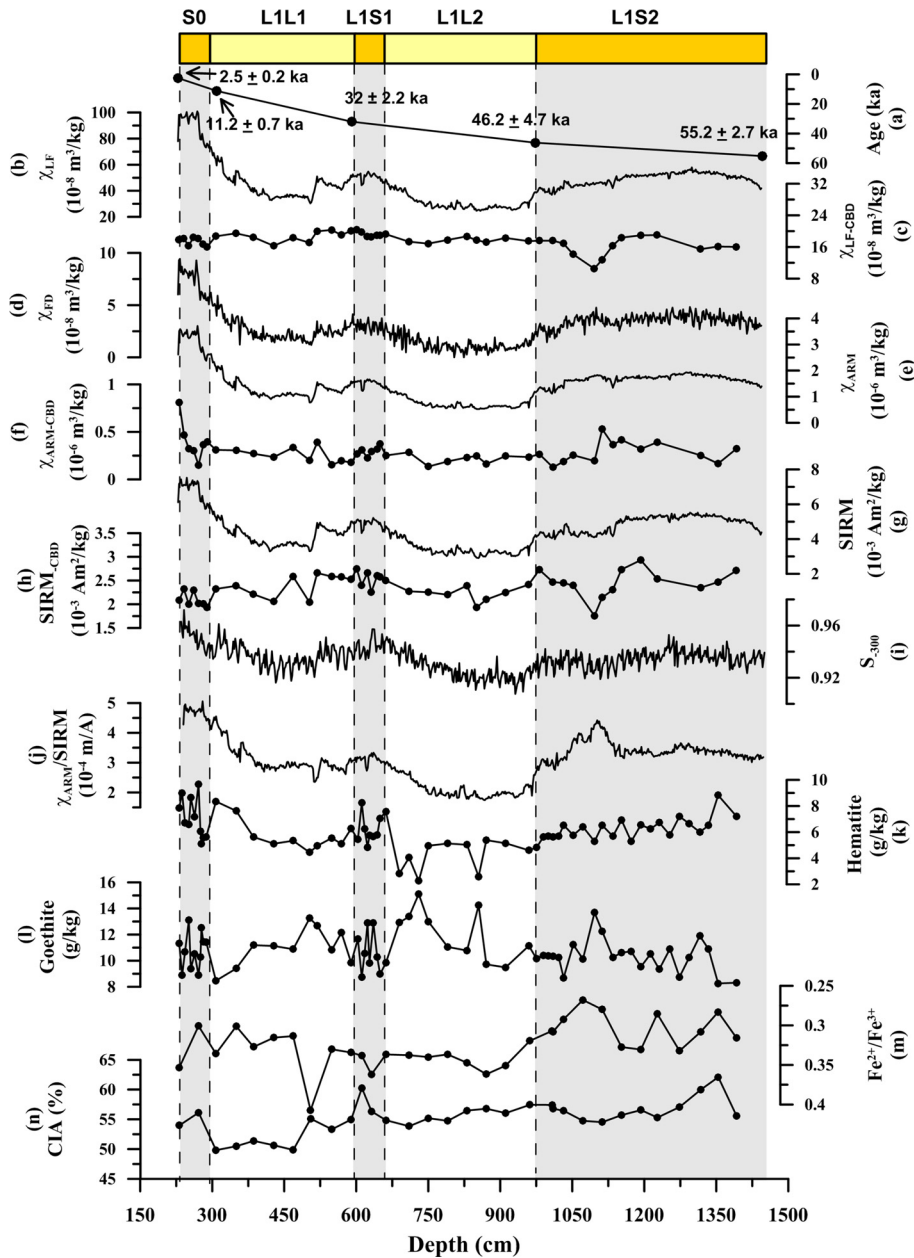


**Fig. 2.** Stratigraphic profile, and magnetic and geochemical depth series from the Ganzi loess: (a) OSL ages; (b) magnetic susceptibility ( $\chi_{LF}$ ); (c) post-CBD  $\chi_{LF-CBD}$ ; (d) frequency-dependent magnetic susceptibility ( $\chi_{FD}$ ); (e) susceptibility of anhysteretic remanent magnetization ( $\chi_{ARM}$ ); (f) post-CBD  $\chi_{ARM-CBD}$ ; (g) saturation isothermal remanent magnetization (SIRM); (h) post-CBD  $SIRM_{-CBD}$ ; (i)  $S_{-300}$  ratio; (j)  $\chi_{ARM}/SIRM$ ; (k) hematite concentration; (l) goethite concentration; (m)  $Fe^{2+}/Fe^{3+}$  ratio, and (n) CIA value.

precipitation (June to September) on average accounting for  $\sim 71\%$  of the annual total. The mean annual temperature is  $10^\circ C$  (1971 to 2000), reaching a maximum of  $23^\circ C$  in July and a minimum of  $-5.5^\circ C$  in January. Currently, Luochuan is under the influence of both the summer and winter components of the East Asian monsoon (Fig. 1b).

## 2.2. Methods

### 2.2.1. Mineral magnetic measurements

Mass-specific magnetic susceptibility ( $\chi$ ) was measured using a Bartington Instruments MS2 magnetic susceptibility meter at dual frequencies of 470 Hz ( $\chi_{LF}$ ) and 4700 Hz ( $\chi_{HF}$ ). The absolute frequency-dependent susceptibility is defined as  $\chi_{FD} = \chi_{LF} - \chi_{HF}$ . An anhysteretic remanent magnetization (ARM) was imparted in an alternating field (AF) of 80 mT with a superimposed 50  $\mu T$

bias field and is expressed in terms of a susceptibility ( $\chi_{ARM} = ARM/50 \mu T$ ). An isothermal remanent magnetization (IRM) was acquired in a field of 1 T, after which a backfield of  $-300$  mT was applied. The corresponding forward and backfield IRMs are referred to as the saturation IRM (SIRM) and  $IRM_{-300}$ , respectively. The S-ratio ( $S_{-300}$ ) was calculated as  $S_{-300} = 0.5 * [-IRM_{-300}/SIRM + 1]$  (Bloemendal et al., 1992). All remanences were measured using a 2-G Enterprises Model 760 cryogenic magnetometer at the Institute of Geology and Geophysics, Chinese Academy of Science (IGGCAS), Beijing. First-order reversal curve (FORC) diagrams were measured with a Princeton Measurements Corporation vibrating sample magnetometer (Micromag VSM 3900). For each sample, 150 FORCs were measured with a field step of 1.2–1.5 mT; data were processed using the algorithm of Heslop and Roberts (2012b) with a smoothing factor of 5. Low-temperature  $\chi-T$  curves were measured with an MPMS in an AF of 0.4 mT at two frequencies

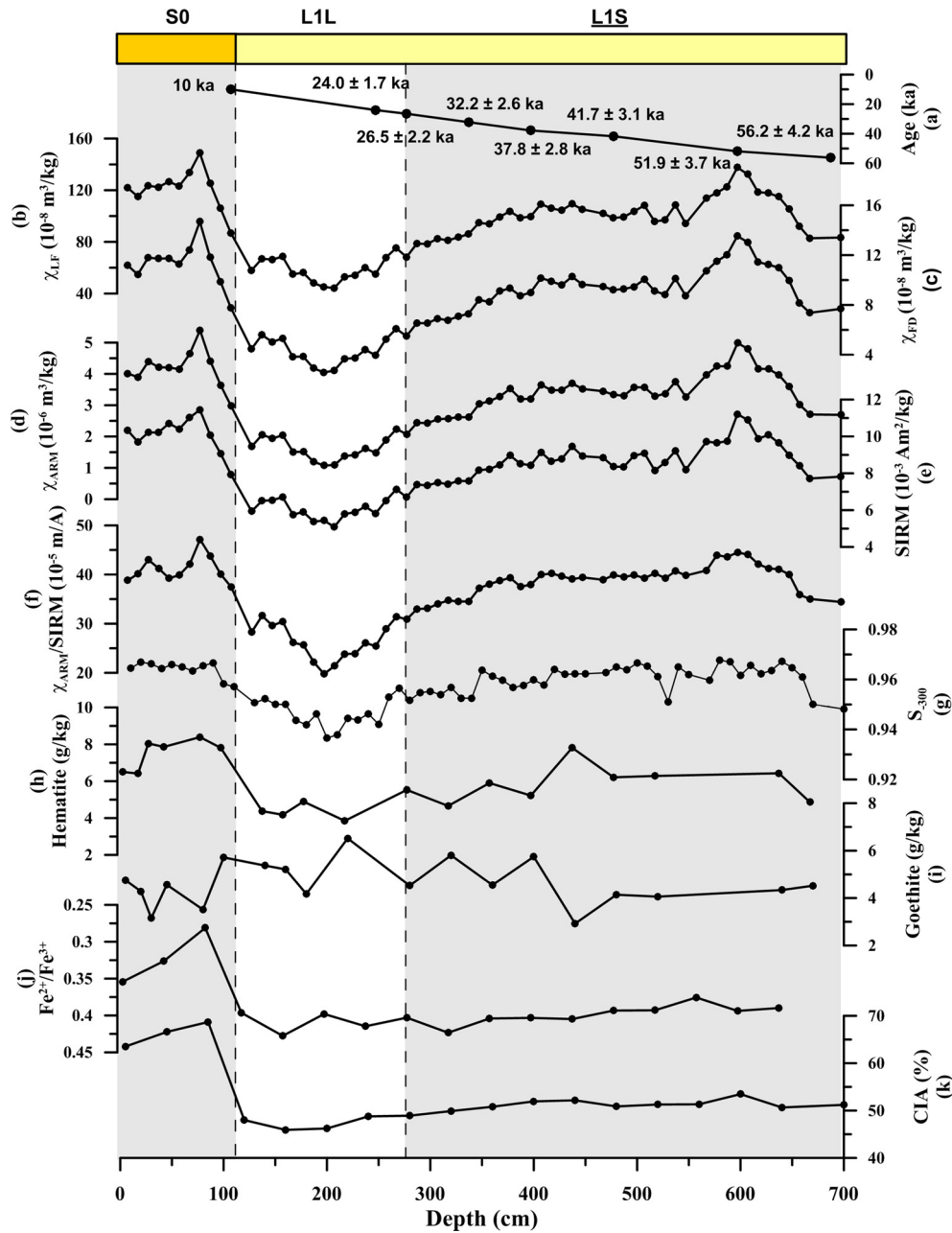


**Fig. 3.** Stratigraphic profile, and magnetic and geochemical depth series from the Luochuan section: (a) OSL ages from Lai (2010); (b)  $\chi_{LF}$ ; (c)  $\chi_{FD}$ ; (d)  $\chi_{ARM}$ ; (e) SIRM; (f)  $\chi_{ARM}/SIRM$ ; (g)  $S_{300}$  ratio; (h) hematite concentration; (i) goethite concentration; (j)  $Fe^{2+}/Fe^{3+}$  ratio, and (k) CIA value. See Fig. 2 caption for parameter descriptions.

(1 Hz and 100 Hz, from 10 K to 300 K). For the low-temperature measurements, frequency-dependent susceptibility is defined as  $\chi_{1\text{ Hz}-100\text{ Hz}}$ .

**2.2.2. Citrate–bicarbonate dithionite extraction**

Fifty representative samples were treated using citrate–bicarbonate dithionite (CBD) extraction (Mehra and Jackson, 1960) (Fig. 2c, f, h). Following the procedure of Torrent et al. (2007), 1.2 g of sodium dithionite was added to 1 g of sample in a sodium citrate solution buffered with sodium bicarbonate. The residual was washed twice with 0.01 M  $CaCl_2$ , twice with deionized water and then dried at 36 °C in preparation for  $\chi_{LF}$ , ARM and SIRM measurements.

**2.2.3. Geochemical measurements**

Major elements were analysed at the Major Elements Laboratory, IGGCAS. Mixtures of bulk sample powder (0.5 g) and  $Li_2B_4O_7$

+  $LiBO_2$  (5 g) were heated and fused into glass disks, which were then analysed by X-ray fluorescence (XRF) spectroscopy with an AXIOS Minerals spectrometer. The analytical uncertainties are 0.1–1%. Loss on ignition (LOI) was measured by heating 0.5 g of powdered sample to 1100 °C for one hour.  $Fe^{2+}$  was measured using the solution Potassium Permanganate Titration method, under the protection of  $CO_2$  gas, after dissolving with  $HF-H_2SO_4$ . Trace element compositions were determined using an inductively coupled plasma mass spectrometer (ICP-MS, ELEMENT, Finnigan MAT) at IGGCAS. The samples were digested in  $HNO_3$  (1:1) and HF under high temperature and pressure. Measurement of two certified reference materials (GSR-1 granite and GSR-3 basalt) indicates that analytical uncertainties for all trace elements in this study are <3%. Five samples from both the Ganzi and Luochuan sections were analysed (Table A.2).

### 2.2.4. X-ray diffraction measurements

X-ray diffraction (XRD) patterns for clay minerals were obtained with a PANalytical diffractometer with monochromatized  $\text{CuK}\alpha$  radiation and a step size of  $0.008^\circ 2\theta$  from  $2^\circ$  to  $35^\circ$  applied to oriented mounts of non-calcareous clay ( $<2 \mu\text{m}$ ) particles separated using the pipette method. Analyses were performed on the two least-weathered L1 samples from the Ganzi and Luochuan sections. For XRD measurements, three specimens of air-dried loess (Mg-ethylene-glycol-saturated, and K-saturated after heating for 2 h at  $550^\circ\text{C}$ ) were analysed. Identification and semi-quantification of clay minerals was made following Z.F. Liu et al. (2010). Illite crystallinity (IC) was also obtained from the half-height width of the  $10 \text{ \AA}$  peak on the ethylene-glycol curve.

## 3. Results

All results shown in figures in this paper that have not been previously published are uploaded into the PANGAEA database (<http://doi.pangaea.de/10.1594/PANGAEA.836298>).

### 3.1. Rare Earth Element (REE) and clay composition of Ganzi loess

Rare earth elements have extremely low mobility and their characteristic features, including Eu anomalies and fractionation of light REEs to heavy REEs, represent compositional differences related to sediment origin. Therefore, REEs and related ratios are widely used as reliable tracers of parent material (Ferrat et al., 2011; Taylor and McLennan, 1985; Zhang et al., 2009). In this study, REE concentrations were normalized to post-Archean Australian shale (PAAS; Taylor and McLennan, 1985; indicated by a subscript 'P'), which has proved to be more effective when comparing REE patterns (Ferrat et al., 2011; Zhang et al., 2009). Eu-anomalies  $(\text{Eu}/\text{Eu}^*)_{\text{P}}$  are defined as  $\text{Eu}_{\text{P}}/\sqrt{\text{Sm}_{\text{P}} * \text{Gd}_{\text{P}}}$ . The Luochuan and Ganzi loess are clearly separated on bivariate plots of  $\text{Y}/\text{Tb}_{\text{P}}$  versus  $(\text{Eu}/\text{Eu}^*)_{\text{P}}$  and  $\text{Y}/\Sigma\text{REE}$  versus  $(\text{La}/\text{Yb})_{\text{P}}$ , which remove dilution effects of certain minerals and are only weakly size-dependent (Ferrat et al., 2011). Values from the Luochuan section are located close to published CLP and Chinese desert values, while Ganzi samples only overlap with Tibetan soils (Fig. 4a, b). Li, Ni, Zr, Rb and Cs are strongly enriched in the Ganzi loess (Table A.2), which is also observed in Tibetan loess (Sun et al., 2007).

Clay mineral assemblages for the least weathered samples from Ganzi and Luochuan consist mainly of illite, kaolinite and chlorite (Fig. 4c). Smectite is not detectable in the Ganzi loess, but accounts for 4.6% of clays in the Luochuan loess. Smectite is typically formed from basic volcanic rocks in alkaline environments. Geological investigations indicate that the Tibetan Plateau is largely covered by Mesozoic limestones, siltstones, shales and weakly metamorphosed felsic rocks, while surface soils from arid northwestern inland China are dominated by Pre-Cambrian to Paleozoic volcanic and strongly mafic metamorphosed rocks (Sun et al., 2008; Yang et al., 2010). Additionally, illite in the Ganzi loess is more crystalline than at Luochuan (IC value: 0.213 and 0.244, respectively), which likely indicates that it formed in a colder and drier environment, such as the Tibetan Plateau. Therefore, differences in clay mineral compositions provide evidence that the Chuanxi loess originates from the interior of the Tibetan Plateau.

### 3.2. Stratigraphic variations of magnetic parameters

#### 3.2.1. Ferrimagnetic minerals

Relative abundances of soft ferrimagnetic and hard antiferromagnetic minerals are commonly quantified using the  $S_{-300}$  ratio (Bloemendal et al., 1992; Evans and Heller, 2003). The Ganzi and Luochuan sections have mean  $S_{-300}$  values of 0.93 and 0.96, respectively (Fig. 2i and Fig. 3g). This demonstrates that ferrimagnetic minerals are magnetically dominant in both sections.

In both sections, the Holocene soil has the highest  $\chi_{\text{LF}}$ ,  $\chi_{\text{FD}}$ ,  $\chi_{\text{ARM}}$  and SIRM values (Fig. 2b, d, e, g and Fig. 3b, c, d, e), which indicate the highest concentrations of ferrimagnetic minerals. However, while subpaleosol layers (L1S) in the last glacial portion of the Luochuan section are magnetically strong (Fig. 3b, c, d, e), the two corresponding layers at Ganzi are not as significantly magnetically enhanced as at Luochuan (Fig. 2b, d, e, g). Moreover, mean values of  $\chi_{\text{LF}}$ ,  $\chi_{\text{FD}}$ ,  $\chi_{\text{ARM}}$  and SIRM for the Ganzi section are  $45.2 \times 10^{-8} \text{ m}^3/\text{kg}$ ,  $2.9 \times 10^{-8} \text{ m}^3/\text{kg}$ ,  $1.4 \times 10^{-6} \text{ m}^3/\text{kg}$  and  $4.5 \times 10^{-3} \text{ Am}^2/\text{kg}$ , respectively, which are approximately half those at Luochuan ( $94.4 \times 10^{-8} \text{ m}^3/\text{kg}$ ,  $8.5 \times 10^{-8} \text{ m}^3/\text{kg}$ ,  $3.1 \times 10^{-6} \text{ m}^3/\text{kg}$  and  $8.3 \times 10^{-3} \text{ Am}^2/\text{kg}$ , respectively). Nevertheless, a consistent linear relationship is observed between  $\chi_{\text{LF}}$ ,  $\chi_{\text{ARM}}$ , SIRM and  $\chi_{\text{FD}}$  (Fig. 5a, b, c), although the data from Ganzi are more scattered. This consistency implies that pedogenic formation of SP/SD magnetite/maghemite accounts for most of the magnetic variability. Variations in detrital mineral input may contribute more to the magnetic properties of the Ganzi loess, which would explain the greater scatter for the Ganzi data compared to CLP correlatives. The observed linear relationship breaks down at low  $\chi_{\text{FD}}$  values ( $< 3 \times 10^{-8} \text{ m}^3/\text{kg}$ ) in the Ganzi loess. Instead,  $\chi_{\text{LF}}$ ,  $\chi_{\text{ARM}}$  and SIRM remain relatively constant, while  $\chi_{\text{FD}}$  starts to gradually increase (Fig. 5a, b, c insets).

Detrital magnetic minerals have previously been characterized using the linear intercepts of various magnetic parameters with respect to  $\chi_{\text{FD}}$  (Deng, 2008; Forster et al., 1996; Liu et al., 2004a, 2004b). These intercepts are designated as  $\chi_{\text{LF0}}$ ,  $\chi_{\text{ARM0}}$ ,  $\text{SIRM}_0$ , etc. (Table 1).  $\chi_{\text{ARM0}}$  is  $35.5 \times 10^{-8} \text{ m}^3/\text{kg}$  for Ganzi and only  $9.1 \times 10^{-8} \text{ m}^3/\text{kg}$  for Luochuan,  $\text{SIRM}_0$  is  $2.9 \times 10^{-3} \text{ Am}^2/\text{kg}$  for Ganzi and  $3.7 \times 10^{-3} \text{ Am}^2/\text{kg}$  for Luochuan, which indicates more SD-like and less coarse detrital magnetic minerals in Ganzi loess.

Detrital magnetic minerals can be also represented by magnetic properties after CBD treatment. During CBD treatment, pedogenic fine-grained iron oxides, including maghemite, magnetite, hematite and goethite are preferentially dissolved, leaving mainly coarse-grained eolian magnetite and titanomagnetite (Deng et al., 2005; Hu et al., 2013; Hunt et al., 1995; Singer et al., 1995). Thus, material with lower  $\chi_{\text{LF}}$  and SIRM in the upper part of subpaleosol L1S2 after CBD treatment may indicate a localized drastic reduction in coarse eolian magnetite input (Fig. 2c, h).

#### 3.2.2. Hematite and goethite

Quantification of hematite and goethite was made using DRS (detailed procedures are described in Torrent et al., 2007). Depth distributions of hematite and goethite are shown in Fig. 2k, l and Fig. 3h, i. In general, the Ganzi and Luochuan sections have similar average hematite concentrations (6.07 and 5.87 g/kg for Luochuan and Ganzi, respectively) with lower values in loess and higher values in paleosols. However, during the last glaciation, the Luochuan section has consistently lower hematite concentrations. In contrast, the average goethite concentration at Ganzi is more than twice that of Luochuan (10.9 g/kg and 4.63 g/kg, respectively). At neither section is there a correlation between goethite and  $\chi_{\text{FD}}$  (Fig. 5f), which probably suggests that goethite formation is independent of ferrimagnetic nanoparticle production (Q.S. Liu et al., 2012). Hematite is positively correlated to  $\chi_{\text{FD}}$  at Luochuan, which is consistent with the results of Torrent et al. (2007) (Fig. 5e). In the Ganzi section, only the Holocene soil and subloess L1L1 have comparable hematite- $\chi_{\text{FD}}$  correlations, which indicates a similar magnetic enhancement mechanism in which ferrimagnetic minerals formed during transformation from ferrihydrite to hematite (Torrent et al., 2007). For L1S1 and L1S2, hematite concentrations are variable (from 5 to 9 g/kg) while  $\chi_{\text{FD}}$  has relatively low values ( $\sim 4 \times 10^{-8} \text{ m}^3/\text{kg}$ ) (Fig. 5e); L1L2 samples have both low  $\chi_{\text{FD}}$  and low hematite concentrations. These results indicate that

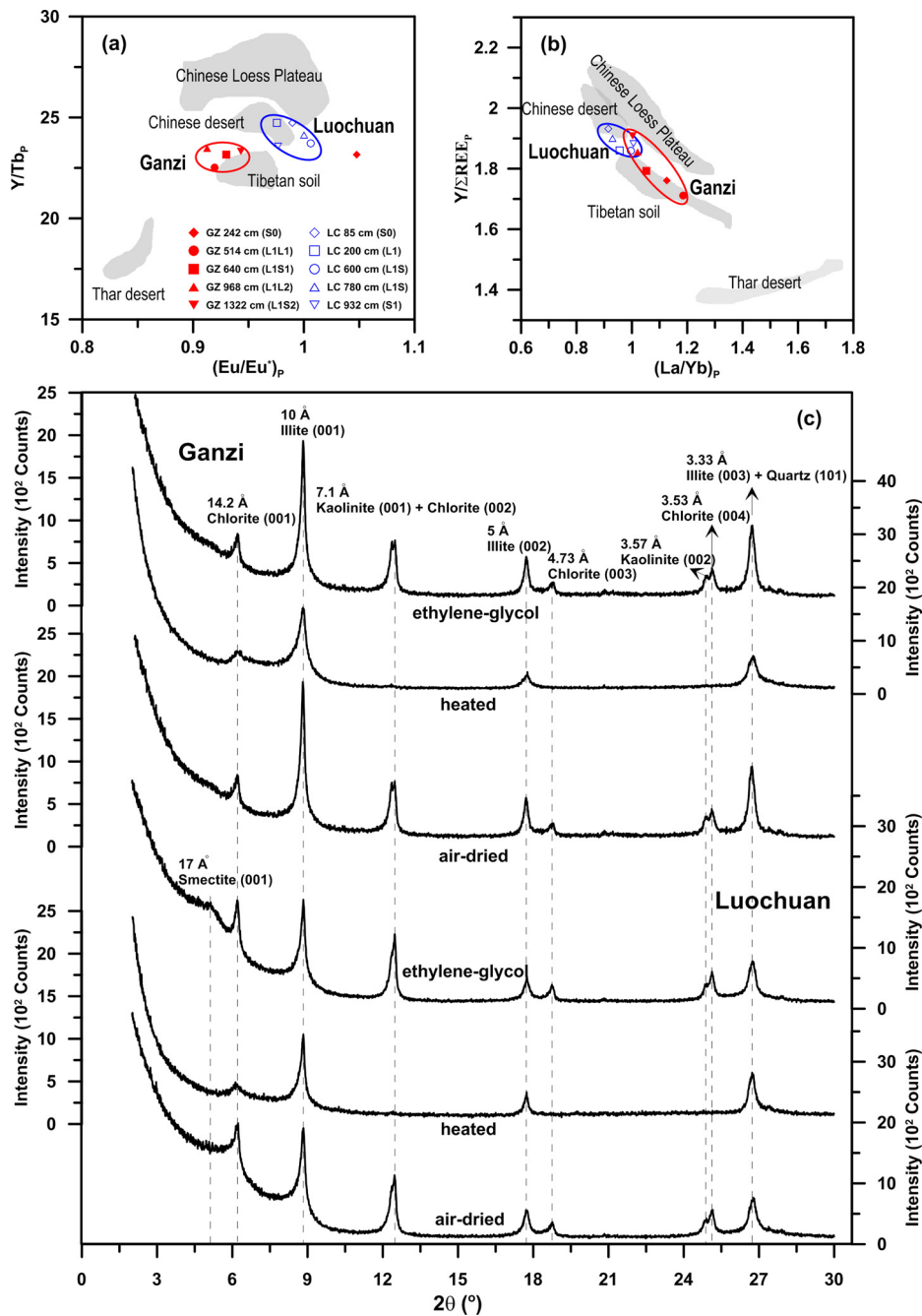


**Fig. 4.** (a) Bivariate plot of  $Y/Tb_p$  versus  $(Eu/Eu^*)_p$ , modified from Fig. 10 of Ferrat et al. (2011). (b) Bivariate plot of  $Y/\Sigma REE_p$  versus  $(La/Yb)_p$ , modified from Fig. 10 of Ferrat et al. (2011). The P subscript indicates that the values are normalized to PAAS. (c) X-ray diffractograms for the least weathered samples from L1 in the Ganzi and Luochuan sections. Three typical results for air-dried, ethylene-glycol saturated and heated conditions are shown. Luochuan and Ganzi loess are clearly separated on the bivariate plots and smectite is only detected in the Luochuan sample, which indicates different origins for the Luochuan and Ganzi loess.

different pedogenic processes must be involved in producing and transforming antiferromagnetic and ferrimagnetic minerals in the Ganzi loess.

### 3.2.3. Magnetic grain size

The  $\chi_{ARM}/SIRM$  ratio provides a grain size indicator for ferrimagnetic minerals in well dispersed sediments, which peaks in the SD range and then decreases with increasing grain size (Maher, 1988). High  $\chi_{ARM}/SIRM$  is observed for paleosol layers from both Ganzi and Luochuan (Fig. 2j and Fig. 3f), which indicates a finer grain size distribution. The upper part of subpaleosol L1S2 at Ganzi has  $\chi_{ARM}/SIRM$  values as high as in the Holocene

soils. A nonlinear relationship exists between  $\chi_{ARM}/SIRM$  and  $\chi_{FD}$  (Fig. 5d) and a second-order polynomial fit is used to estimate  $(\chi_{ARM}/SIRM)_0$ , which represents the  $\chi_{ARM}/SIRM$  value of parent material.  $(\chi_{ARM}/SIRM)_0$  is  $1.6 \times 10^{-4}$  m/A and  $1.1 \times 10^{-4}$  m/A for Ganzi and Luochuan, respectively, which indicates a finer grain size for the eolian input at Ganzi.

FORC diagrams provide a means of identifying magnetic mineral components, their domain state, and magnetic interactions (Pike et al., 1999, 2001; Roberts et al., 2000, 2006; Egli et al., 2010). In Fig. 6, the main part of the FORC distributions for paleosol samples (Fig. 6a, c, e, f, h) has a ridge-like component at  $B_0 = 0$  mT that intersects the origin of the FORC diagram. This indicates the

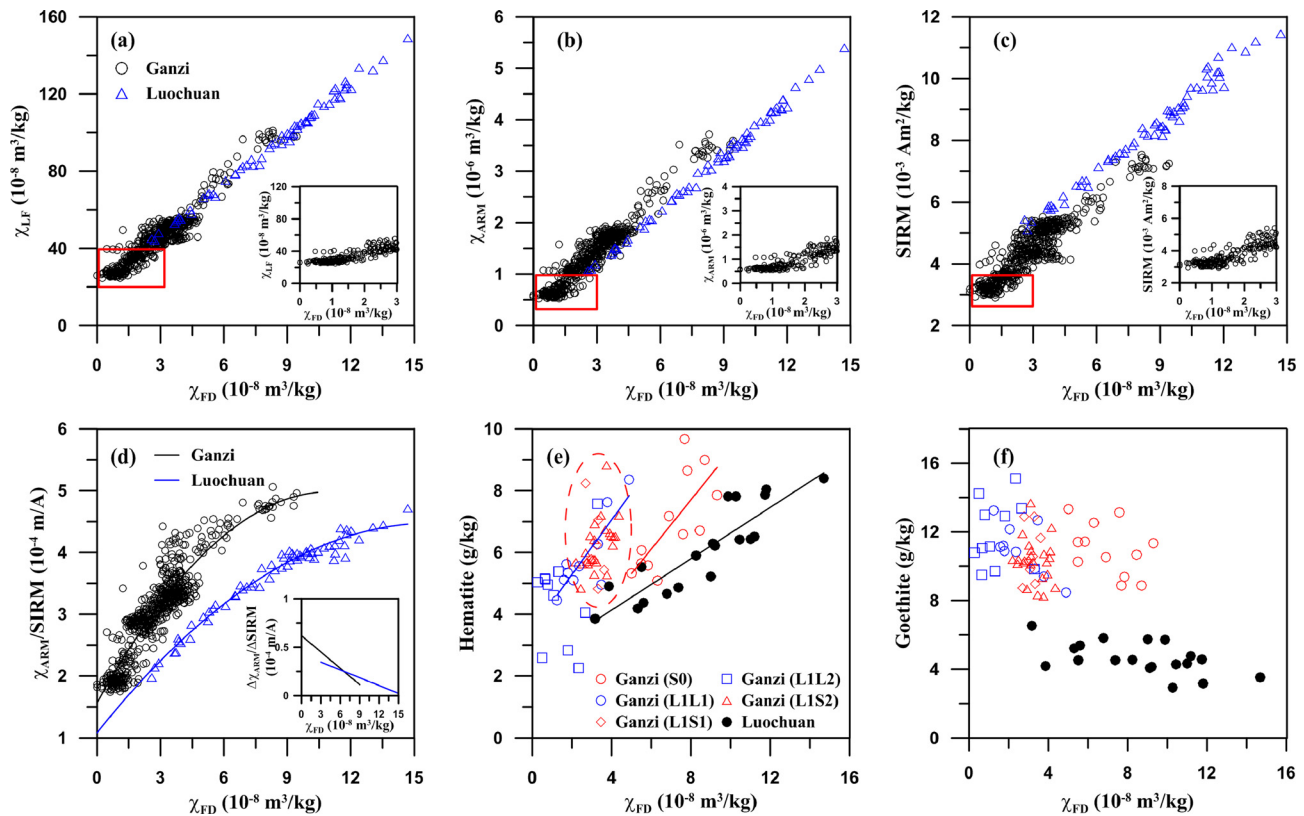


**Fig. 5.** Relationship between (a)  $\chi_{LF}$  versus  $\chi_{FD}$ ; (b)  $\chi_{ARM}$  versus  $\chi_{FD}$ ; (c) SIRM versus  $\chi_{FD}$ ; (d)  $\chi_{ARM}/SIRM$  versus  $\chi_{FD}$ ; (e) hematite versus  $\chi_{FD}$  and (f) goethite versus  $\chi_{FD}$  for both the Ganzi and Luochuan sections. The inset panels in (a), (b), (c) are enlargements for the region with low  $\chi_{FD}$  values. Black and blue curves in (d) represent the best second-order polynomial fitting lines for Ganzi and Luochuan, respectively. The inset panel in (d) is for  $\Delta\chi_{ARM}/\Delta SIRM$  versus  $\chi_{FD}$ . Blue, red and black lines in (e) represent the linear regression between hematite and  $\chi_{FD}$  of Ganzi L1L1 samples, Ganzi Holocene paleosol samples and Luochuan samples, respectively. Red dashed circle highlights the subpaleosol samples. The corresponding coefficients of determination ( $R^2$ ) are 0.71, 0.54 and 0.78, respectively. (For interpretation of the references to color in this figure legend, the reader is referred to the web version of this article.)

**Table 1**

Mineral magnetic parameters for eolian contributions at Luochuan and Ganzi over the last glacial cycle.

Parameters	Ganzi <sup>b</sup>	Luochuan <sup>b</sup>
$\chi_{LF0}$ ( $10^{-8}$ m <sup>3</sup> /kg)	$20.07 \pm 0.84$	$21.53 \pm 1.49$
Slope- $\chi_{LF}$	$8.72 \pm 0.23$	$8.61 \pm 0.16$
$\chi_{ARM0}$ ( $10^{-8}$ m <sup>3</sup> /kg)	$35.48 \pm 3.15$	$9.07 \pm 5.50$
Slope- $\chi_{ARM}$ <sup>a</sup>	$36.64 \pm 0.86$	$35.68 \pm 0.59$
SIRM <sub>0</sub> ( $10^{-3}$ Am <sup>2</sup> /kg)	$2.90 \pm 0.07$	$3.70 \pm 0.18$
Slope-SIRM ( $10^4$ A/m) <sup>a</sup>	$5.38 \pm 0.19$	$5.42 \pm 0.20$
$(\chi_{ARM}/SIRM)_0$ ( $10^{-4}$ A/m)	$1.57 \pm 0.07$	$1.08 \pm 0.18$

<sup>a</sup> Slope- refers to the gradient of linear correlation among magnetic parameters and  $\chi_{FD}$ . For example, Slope- $\chi$  refers to the gradient of the linear correlation between  $\chi_{LF}$  and  $\chi_{FD}$ .

<sup>b</sup> Uncertainties are given at the 95% significance levels.

dominance of magnetically non-interacting SD and thermally relaxed SP particles near the SP/SD threshold size (Roberts et al., 2000; Pike et al., 2001). Some paleosol samples have a weaker part of the FORC distribution with greater vertical spread and triangular contours that are likely to be due to a coarser PSD component (Roberts et al., 2000; Muxworthy and Dunlop, 2002) (Fig. 6c, h). FORC diagrams for loess samples have relatively large vertical spread (Fig. 6b, d, g), which indicates the presence of both fine SP/SD particles and coarser PSD particles in both sections. Corresponding hysteresis parameters are also shown on Fig. 6. Paleosols have higher  $M_{rs}/M_f$  and lower  $B_{cr}/B_c$  values than loess, which is consistent with  $\chi_{ARM}/SIRM$  ratios and FORC distributions, which also indicate a finer grain size distribution in the paleosols.

Grain size distributions for SP particles can be determined from low-temperature susceptibility curves, which record unblocking

of fine ferrimagnetic particles during warming (Liu et al., 2005; Worm et al., 1991). In Fig. 7a, c, d,  $\chi_{1\text{ Hz}-100\text{ Hz}}$  reaches a maximum between 150 and 200 K in Ganzi paleosols, while for Luochuan paleosols, it monotonically increases up to 250 K with a smaller slope at 300 K. Following Liu (2004) and Liu et al. (2005), unblocking results were converted into a grain size distribution (Fig. 7g, h), which was fitted with a lognormal distribution between 10 nm and 25 nm and extrapolated to 80 nm. Peaks of the SP grain size distribution occur at  $\sim 20.0$  to  $\sim 20.7$  nm and  $\sim 23.0$  to  $\sim 24.8$  nm for the Ganzi and Luochuan samples, respectively. The corresponding distribution widths are  $\sim 0.44$  to  $\sim 0.51$  and  $\sim 0.56$  to  $\sim 0.65$ , respectively.

### 3.3. Geochemical results

Chemical index of alteration (CIA) values and  $\text{Fe}^{2+}/\text{Fe}^{3+}$  ratios provide a broad outline of weathering intensity and degree of transformation of Fe-bearing minerals into iron oxides. For the Luochuan section, the Holocene soil has high CIA values and low  $\text{Fe}^{2+}/\text{Fe}^{3+}$  ratios, which suggests intense chemical weathering and ferric iron oxide formation (Fig. 3j, k). In contrast, during the last glacial period, the Luochuan loess has consistently low CIA values and high  $\text{Fe}^{2+}/\text{Fe}^{3+}$  ratios, which suggests weak weathering intensity. However, for the Ganzi section, weathering and iron oxide production was significantly enhanced in the last glacial period, particularly in subpaleosol L1S2, as indicated by high CIA and low  $\text{Fe}^{2+}/\text{Fe}^{3+}$  values (Fig. 2m, n). Moreover, the Ganzi loess has higher overall CIA values and lower  $\text{Fe}^{2+}/\text{Fe}^{3+}$  ratios than the Luochuan section, which indicates stronger weathering intensity.

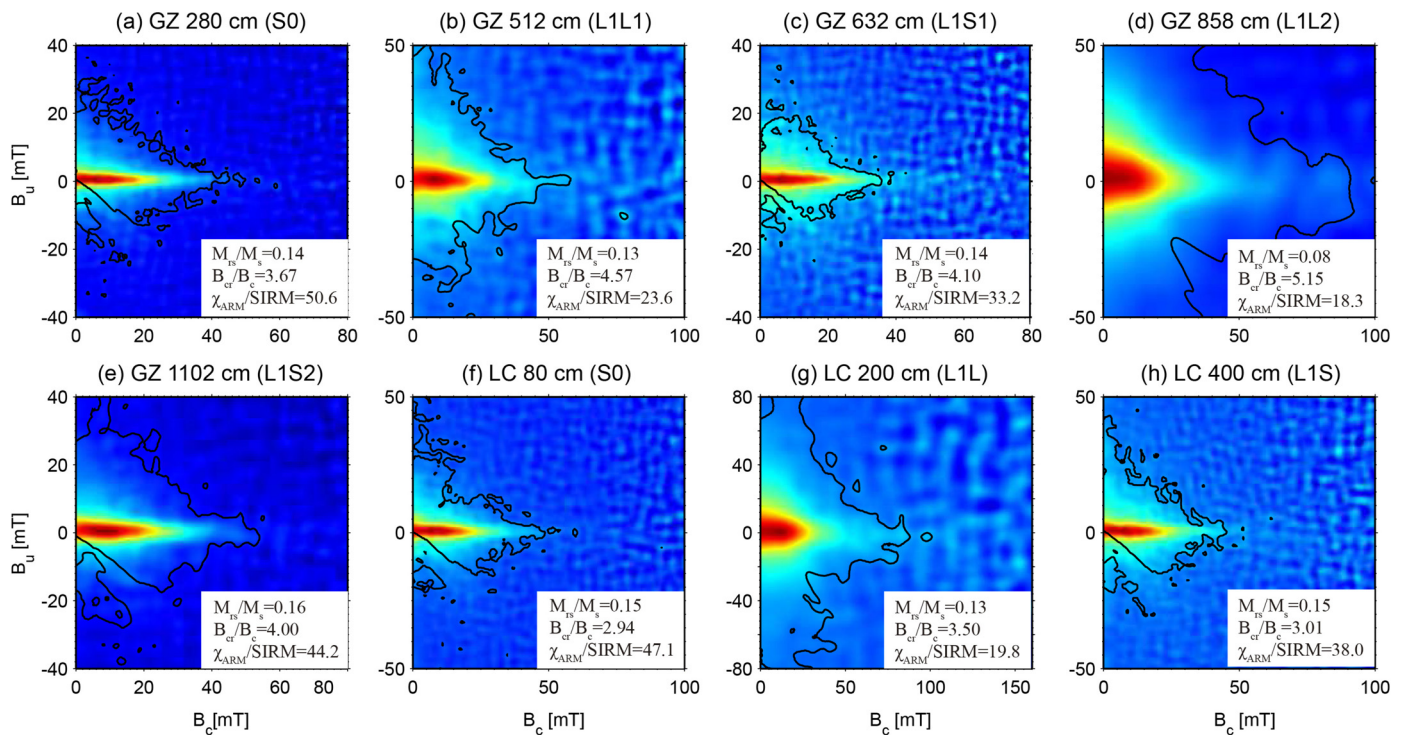


**Fig. 6.** FORC diagrams for typical samples from the Ganzi (a–e) and Luochuan (f–h) sections. The thick contour line indicates regions of the FORC distribution that are significant at the 95% significance level (Heslop and Roberts, 2012b). The units for values of  $\chi_{ARM}/SIRM$  are  $10^{-5}$  m/A.

## 4. Discussion

### 4.1. Parent material and magnetic properties of loess

Trace elements and clay minerals help to discriminate different source areas for the Ganzi and CLP loess. The Tibetan Plateau is the major eolian source for the Chuanxi loess, which is consistent with observations of eolian features and fluvial/glacial surface textures in the Ganzi loess (Fang, 1994; Fang et al., 1996; Qiao et al., 2006; Wang et al., 2003). In contrast, CLP loess source regions include the Badain Juran and Tengger deserts, and the Qaidam basin in northern China and the Gobi Desert in southern Mongolia (Chen et al., 2007; Sun et al., 2008). These provenance differences could give rise to different iron sources; eolian iron-bearing minerals will, thus, influence soil magnetism.

The influence of initial Fe input was discussed by Dearing et al. (1996), who reported a positive, albeit weak, correlation between total Fe and soil magnetic susceptibility. Maher (1998) provided an alternative interpretation, however, concluding that Fe input will rarely be a limiting factor. Total Fe at Ganzi is comparable to that at Luochuan (3.2% and 3.25%, respectively, from major element analysis), but values of  $\chi_{LF}$ ,  $\chi_{FD}$ ,  $\chi_{ARM}$  and SIRM are around half those observed at Luochuan (Figs. 2, 3). Thus, our data favour the explanation of Maher (1998) that higher Fe content does not necessarily result in stronger ferrimagnetism and that specific pedogenic processes, rather than total Fe supply, have a greater influence on ferrimagnet formation.

Provenance differences will also change the composition of detrital magnetic mineral assemblages. Higher  $\chi_{ARM0}$  and lower SIRM<sub>0</sub> values indicate more SD-like and less coarse detrital magnetic minerals in Ganzi loess (Table 1). The concentration-independent ratio  $(\chi_{ARM}/SIRM)_0$  also indicates a finer grain size for the eolian input to Ganzi loess. The  $\chi_{ARM}/SIRM$  peak in subpaleosol L1S2 at Ganzi corresponds to a sudden decrease in post-CBD  $\chi_{LF}$  and SIRM (Fig. 2c, j), which also indicates that a sharp decrease in coarser eolian ferrimagnetic particles is responsible for the finer

grain sizes observed in L1S2. Stronger source area weathering is a possible explanation for those observations. Fang (1994) analysed more than 2500 quartz sands from different loess sections on the Tibetan Plateau and surrounding areas, including the western CLP. The concentration of quartz sands altered by chemical weathering increased toward the interior of the Tibetan Plateau. This indicates that chemical weathering on the Tibetan Plateau is generally stronger than in the northern Asian deserts, which is likely to produce finer detrital magnetic iron oxides. Sorting during wind transportation is another possible mechanism with westerlies dominating the Tibetan Plateau in winter. Finer particles are more likely to be dispersed higher into the atmosphere, which means fine dust can be transported by upper-level westerlies (Pye, 1995). Additionally, the intrinsic properties of dust source areas could result in more SD particles and finer magnetic particles in the loess parent material. However, both sections have large source areas, so detrital materials are expected to be thoroughly mixed before deposition, which suggests that the initial composition of source material is not likely to play a dominant role.

The Ganzi loess also has high goethite contents compared to contemporaneous CLP loess (Table 1, values from Deng, 2008). Goethite formation is favoured by cool and relatively humid climates, such as in the Chuanxi Plateau and Tibet, rather than the dry climates of northern Chinese deserts. Additionally, the arid northwestern interior of China is dominated by Paleozoic and older rocks, which usually have lower goethite contents (Cornell and Schwertmann, 2003).

Despite the discussed influences of eolian input on magnetic records, the Ganzi loess has still been magnetically enhanced at similar levels to the CLP loess; specifically, maghemite nanoparticles formed by *in situ* pedogenesis give rise to strong paleosol magnetism, which is characterized by a linear relationship between  $\chi_{LF}$ ,  $\chi_{FD}$ ,  $\chi_{ARM}$  and SIRM (Fig. 5a, b, c). This similarity indicates that pedogenic processes and their controlling climate

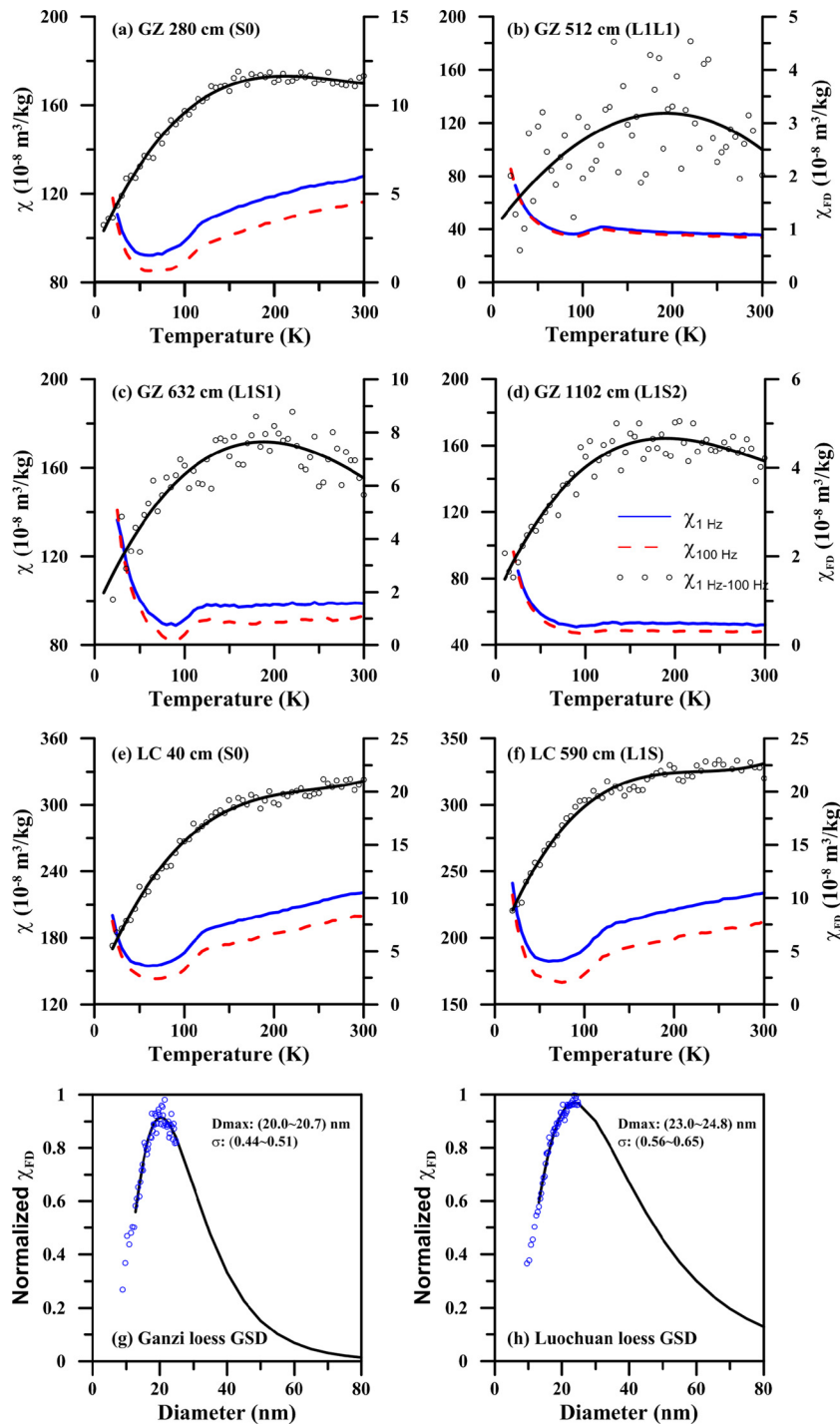


**Fig. 7.** Low-temperature magnetic susceptibility for Ganzi (a–d) and Luochuan (e–f). The frequency-dependence of magnetic susceptibility ( $\chi_{1 \text{ Hz}-100 \text{ Hz}}$ , open symbols) is fitted with a third-order polynomial (black line). (g–h) Grain size distribution (GSD) of SP/SD ferrimagnetic particles for Ganzi (g) and Luochuan loess (h). Blue circles are the original data and the black lines are the lognormal fits.  $D_{\text{max}}$  and  $\sigma$  represent the grain size distribution in terms of the maximum  $\chi_{1 \text{ Hz}-100 \text{ Hz}}$  and the width of the lognormal distribution, respectively. The range of  $D_{\text{max}}$  and  $\sigma$  is calculated for the 95% confidence level. Room temperature  $B_c$  is set to be 22.5 mT without considering thermal fluctuations.  $M_s$  values for maghemite are set at 380 kA/m. (For interpretation of the references to color in this figure legend, the reader is referred to the web version of this article.)

factors, rather than eolian input, are the major factors that control iron oxide formation and transformation.

#### 4.2. Pedogenic pathways of iron oxides and magnetic properties of loess

##### 4.2.1. Formation of SP ferrimagnetic particles

Although loess from Ganzi and Luochuan yields almost identical linear relationships between  $\chi_{FD}$  and  $\chi_{LF}$ , and between  $\chi_{ARM}$  and SIRM, it appears that the particles that account for the initial

$\chi_{FD}$  increase exert little influence on  $\chi_{LF}$ ,  $\chi_{ARM}$ , and SIRM, that results in a plateau near the origin of Fig. 5a, b, c (inset panels).  $\chi_{FD}$  is sensitive to grain size changes for particles around the SP/SD boundary (Worm, 1998; Liu, 2004), therefore, this behaviour suggests that the initial  $\chi_{FD}$  increase probably resulted from a change in grain size distribution rather than a change in ferrimagnetic mineral concentration. Data from weakly weathered loess (L1L2) fall on this plateau, therefore, it is reasonable to propose that when fine pedogenic particles start to form, their grain size increases

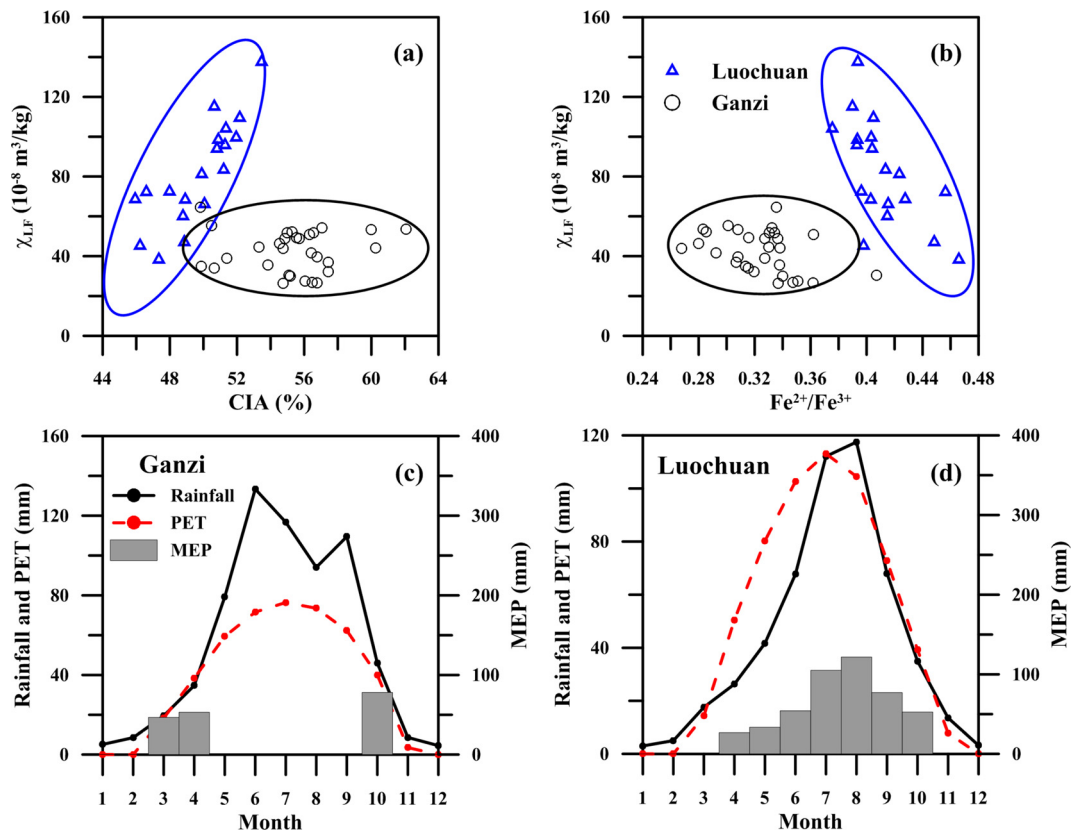


**Fig. 8.** Bivariate relationship between (a)  $\chi_{LF}$  and CIA; (b)  $\chi_{LF}$  and  $Fe^{2+}/Fe^{3+}$  for samples from the last glacial, shown with the monthly distribution of rainfall, PET and MEP for the Ganzi (c) and Luochuan (d) sections.

gradually toward the SP/SD threshold size, causing a considerable increase in  $\chi_{FD}$  with only minor influence on  $\chi_{LF}$ ,  $\chi_{ARM}$ , and SIRM. Therefore, initial growth of SP particles is recorded in Ganzi loess. Most CLP loess does not record this initial growth phase because loess weathering is too weak and chemical weathering in paleosols reaches a stable state due to carbonate leaching and addition of calcareous dust, which produces a more uniform ferrimagnetic grain size distribution (see also Q.S. Liu et al., 2010).

From the estimated grain size distribution of SP particles (Fig. 7), we infer that the grain size dispersion at Ganzi is significantly smaller than at Luochuan. Additionally, the distribution mode at Ganzi is shifted to smaller grain sizes ( $\sim 20$  nm), which indicates that production of SP particles is limited to a narrower and finer grain size range than at Luochuan. At the initial stage of pedogenesis, a finer grain size composition of pedogenic ferrimagnetic minerals is indicated with  $\Delta\chi_{ARM}/\Delta SIRM$  higher at Ganzi than Luochuan (Fig. 5d).

Several factors could be responsible for finer SP particles at Ganzi. Silicates, phosphates and organics in soil solution may interfere with iron oxide crystal growth because they interact with crystal surfaces (Cornell and Schwertmann, 2003). Synthetic experiments demonstrate that the size of nanoscale magnetite precipitated in aqueous solution decreases with ionic strength due to the lower surface tension of particles in these milieus (Vayssières et al., 1998). The concentration of organic matter, especially organic acids, will also have an effect on magnetite particle size via surface charge effects. For example, a greater amount of either humate or citrate can result in smaller magnetic particles by preventing aggregation (Hajdú et al., 2009). All of these factors could account for the finer SP particles in the Chuanxi loess because compared to the warmer climate on the CLP, colder and more humid conditions (higher soil moisture, as discussed in Section 4.3) would favour a higher concentration of organic matter. Production of fine SP parti-

cles may also not be independent of parent material. A more felsic provenance is potentially responsible for producing finer SP particles by providing Al sources such as feldspars, micas, kaolinite and gibbsite. Specifically, a higher Al/(Al + Fe) ratio will accompany a reduction in unit cell size for maghemite in soils (Fontes and Weed, 1991; Schwertmann and Fechter, 1984).

#### 4.2.2. Transformation of ferrimagnetic minerals to antiferromagnetic minerals

CIA and  $Fe^{2+}/Fe^{3+}$  ratios indicate an increase in pedogenic intensity in subpaleosol layers at Ganzi during the last glacial period (Fig. 2m, n). The Rb/Sr ratio, which has been used as an indicator of pedogenic intensity due to the differential weathering capacity of the major Rb and Sr host minerals (Chen et al., 1999; Gallet et al., 1996), is also higher at Ganzi (Table A.2). Low Ca contents of the Ganzi loess (5.75% compared to 4.00% for last glacial loess at Luochuan) provide further evidence for more intense carbonate leaching, which is also reflected by its generally darker colour. However,  $\chi_{LF}$ ,  $\chi_{FD}$ ,  $\chi_{ARM}$  and SIRM values for the last glacial subpaleosol layers are only around half those of correlatives at Luochuan (Figs. 2, 3). Therefore,  $\chi_{LF}$  versus CIA and  $Fe^{2+}/Fe^{3+}$  for the two sections are clearly separated (Fig. 8a, b).

Typically, enhanced pedogenic intensity produces magnetic enhancement through neoformation of magnetite/maghemite nanoparticles. However, this mechanism does not always apply due to transformation of strong magnetic components to weak or non-magnetic components. For instance, intense precipitation may lead to strong vertical leaching and gleying, which causes magnetic mineral dissolution (Chlachula, 2003; Guo et al., 2001; Liu et al., 2013; Nawrocki et al., 1996). In the Ganzi section, there is no evidence for excessive waterlogging and strong iron leaching. Therefore, high pedogenic intensity but low ferrimagnetism may have resulted from pedogenic transformation of strongly magnetic

minerals to relatively weakly magnetic minerals, which led to an enhanced ratio of hematite content to  $\chi_{FD}$  in subpaleosols (Fig. 5e).

In soil or sedimentary environments, fine-grained hematite usually forms via chemical transformation of ferrihydrite (Cornell and Schwertmann, 2003), which itself forms by weathering and hydrolysis of primary Fe-bearing minerals (Orgeira et al., 2011; Yang et al., 2013). A recent model suggests that hematite formation in soils via ferrihydrite can produce an intermediate ferrimagnetic phase, but that hematite will eventually replace this intermediate phase with increasing aging (Michel et al., 2010). Such ferrimagnetic mineral transformation to weak antiferromagnetic hematite could explain why weathering during the last glacial resulted in decreased magnetic susceptibility and remanences at Ganzi.

#### 4.3. Soil moisture balance and magnetic enhancement

Precipitation has been recognized as the primary climatic factor that controls the magnetic properties of soils. Strong correlation between MAP and environmental magnetic parameters has been identified (Geiss and Zanner, 2007; Heller et al., 1993; Maher and Thompson, 1991, 1995) and empirical models have been developed to relate precipitation to rock magnetic parameters (Balsam et al., 2011; Liu et al., 2013; Maher et al., 1994), although the statistical robustness of paleoprecipitation predictions from magnetic properties has been questioned (Heslop and Roberts, 2013). According to these models, with elevated rainfall, magnetic parameters will increase until a rainfall threshold of  $\sim 1000$  mm/yr is reached (Liu et al., 2013). Although MAP in the Ganzi region is significantly higher than at Luochuan (660 mm/yr versus 510 mm/yr), the Ganzi loess is ferrimagnetically weaker, as demonstrated by lower  $\chi_{LF}$ ,  $\chi_{ARM}$ , and SIRM values (Fig. 2b, d, e, g). This discrepancy does not appear to fit any previous models that relate magnetic properties to rainfall. Orgeira et al. (2011) proposed that soil water balance, rather than MAP, is the most important factor that controls magnetic enhancement because it will dominate the annual soil ‘wetting’ and ‘drying’ cycle. They constructed a quantitative model to link pedogenic magnetite and soil water balance and defined a new parameter termed the “magnetite enhancement proxy” (MEP) (formula 25.19 in Orgeira et al., 2011) based on rainfall, soil type, vegetation and PET, which is a measure of the ability of the atmosphere to remove water from the surface through evaporation and transpiration, assuming no control on water supply.

We calculated PET and MEP based on 30-yr mean monthly rainfall and temperature data (Fig. 8c, d). Mean monthly data may not be equivalent to the data of Orgeira et al. (2011), but we use such data for comparative purposes. At Ganzi, monthly PET values are lower than rainfall throughout the year, with the largest difference during summer. Based on these calculations, MEP is only non-zero in March, April, October and totals 178 mm/yr. In contrast, PET and rainfall are comparable at Luochuan and magnetite can be produced throughout summer, resulting in a total MEP of 471 mm/yr. The large difference in MEP between Ganzi and Luochuan might explain the low  $\chi_{LF}$ ,  $\chi_{ARM}$ , and SIRM values at Ganzi. Orgeira et al. (2011) proposed that high soil moisture hinders pedogenic magnetite formation, which results in low MEP. However, based on our results from Ganzi and Luochuan, although ferrimagnetism is weaker in Ganzi loess the pedogenic intensity is higher (Fig. 2m, n and Fig. 8a, b) and more hematite is observed when there is less pedogenic maghemite (Fig. 5e). Moreover, initial growth of SP particles is observed in incipient loess samples (Fig. 5a, b, c), which suggests the gradual formation of maghemite with increasing pedogenesis, consistent with a ferrihydrite  $\rightarrow$  ferrimagnetic intermediate phase  $\rightarrow$  hematite transformation (Liu et al., 2008; Michel et al., 2010). Therefore, weak ferrimagnetism is most likely due to the transformation of maghemite to hematite rather than to no magnetite production in high soil moisture periods. We did

not document magnetic iron oxide dissolution in the Ganzi section, which indicates that although soil moisture is relatively higher at Ganzi than Luochuan, appropriate redox conditions for magnetite dissolution were not reached. As a result, we prefer the mechanism that higher soil moisture promotes the pedogenic pathway of ferrihydrite  $\rightarrow$  ferrimagnetic intermediate phase  $\rightarrow$  hematite and results in the generally low ferrimagnetism in Ganzi loess.

## 5. Conclusions

We have presented the first detailed environmental magnetic investigation of the Chuanxi loess from the Tibetan Plateau. By comparing loess from Chuanxi and the CLP, several important conclusions can be drawn concerning the magnetic properties of loess from different climate zones. In contrast to the CLP, the Chuanxi loess originates predominantly from the Tibetan Plateau interior. This provenance difference adds complexity when interpreting magnetic variations in terms of the type, concentration and grain size of eolian magnetic minerals. We also demonstrate the ‘double-edged sword’ nature of pedogenesis. On the one hand, enhanced weathering produces magnetic enhancement in paleosol layers through magnetite/maghemite nanoparticle neof ormation at Luochuan and in the Holocene paleosol at Ganzi. However, high soil moisture, reflected by high MAP and low PET, favours transformation of maghemite to hematite, which leads to the weak ferrimagnetism of the Ganzi loess. Overall, environmental magnetic information recorded by Chinese loess and paleosols represents a complicated response of different pedogenic processes under the combined influence of numerous climate factors. Soil water balance provides a suitable representation of these climate factors.

## Acknowledgements

This work was supported by the Natural Science Foundation of China (41374073, 41025013, 41004023 and 41272202), the “Strategic Priority Research Program” of the Chinese Academy of Sciences (XDB03020102), and the National Basic Research Program of China (2013CB956403). Pengxiang Hu was further supported by the China Scholarship Council ([2013]3009). David Heslop and Andrew P. Roberts were supported by an Australian Research Council Discovery Project (DP110105419). We thank Dr. Chunxia Zhang for assistance in measuring and analysing XRD data. We also thank Dr. Chuan Lu for laboratory assistance and technical support and Prof. José Torrent and Dr. Xiang Zhao for discussions. We are grateful to Ramon Egli, Stefanie Brachfeld, and an anonymous reviewer for their helpful suggestions.

## Appendix A. Supplementary material

Supplementary material related to this article can be found online at <http://dx.doi.org/10.1016/j.epsl.2014.10.035>.

## References

- An, Z.S., 2000. The history and variability of the East Asian paleomonsoon climate. *Quat. Sci. Rev.* 19, 171–187.
- Balsam, W.L., Ellwood, B.B., Ji, J.F., Williams, E.R., Long, X.Y., El Hassani, A., 2011. Magnetic susceptibility as a proxy for rainfall: worldwide data from tropical and temperate climate. *Quat. Sci. Rev.* 30, 2732–2744.
- Begét, J.E., Stone, D.B., Hawkins, D.B., 1990. Paleoclimatic forcing of magnetic-susceptibility variations in Alaskan loess during the Late Quaternary. *Geology* 18, 40–43.
- Bloemendal, J., King, J.W., Hall, F.R., Doh, S.J., 1992. Rock magnetism of Late Neogene and Pleistocene deep-sea sediments: relationship to sediment source, diagenetic processes, and sediment lithology. *J. Geophys. Res.* 97, 4361–4375.
- Boyle, J.F., Dearing, J.A., Blundell, A., Hannam, J.A., 2010. Testing competing hypotheses for soil magnetic susceptibility using a new chemical kinetic model. *Geology* 38, 1059–1062.

- Chen, J., An, Z.S., Head, J., 1999. Variation of Rb/Sr ratios in the loess–paleosol sequences of central China during the last 130,000 years and their implications for monsoon paleoclimatology. *Quat. Res.* 51, 215–219.
- Chen, J., Li, G., Yang, J., Rao, W., Lu, H., Balsam, W., Sun, Y., Ji, J., 2007. Nd and Sr isotopic characteristics of Chinese deserts: implications for the provenances of Asian dust. *Geochim. Cosmochim. Acta* 71, 3904–3914.
- Chen, S., Fang, X.M., Wang, S., 2002. Relation between the loess stratigraphy on the eastern Tibetan Plateau and Indian monsoon. *Mar. Geol. Quat. Geol.* 22, 41–46 (in Chinese).
- Chlachula, J., 2003. The Siberian loess record and its significance for reconstruction of Pleistocene climate change in north-central Asia. *Quat. Sci. Rev.* 22, 1879–1906.
- Chlachula, J., Evans, M.E., Rutter, N.W., 1998. A magnetic investigation of a Late Quaternary loess/paleosol record in Siberia. *Geophys. J. Int.* 132, 128–132.
- Cornell, R.M., Schwertmann, U., 2003. *The Iron Oxides: Structure, Properties, Reactions, Occurrences and Uses*, second ed. Wiley-VCH, Weinheim, Germany.
- Dearing, J.A., Hay, K.L., Baban, S.M.J., Huddleston, A.S., Wellington, E.M.H., Loveland, P.J., 1996. Magnetic susceptibility of soil: an evaluation of conflicting theories using a national data set. *Geophys. J. Int.* 127, 728–734.
- Dekkers, M.J., 1997. *Environmental magnetism: an introduction*. *Geol. Mijnb.* 76, 163–182.
- Deng, C.L., 2008. Paleomagnetic and mineral magnetic investigation of the Baicaoyuan loess–paleosol sequence of the western Chinese Loess Plateau over the last glacial–interglacial cycle and its geological implications. *Geochim. Geophys. Geosyst.* 9, Q04034. <http://dx.doi.org/10.1029/2007gc001928>.
- Deng, C.L., Vidic, N.J., Verosub, K.L., Singer, M.J., Liu, Q.S., Shaw, J., Zhu, R.X., 2005. Mineral magnetic variation of the Jiaodao Chinese loess/paleosol sequence and its bearing on long-term climatic variability. *J. Geophys. Res.* 110, B03103. <http://dx.doi.org/10.1029/2004jb003451>.
- Deng, C.L., Shaw, J., Liu, Q.S., Pan, Y.X., Zhu, R.X., 2006. Mineral magnetic variation of the Jingbian loess/paleosol sequence in the northern Loess Plateau of China: implications for Quaternary development of Asian aridification and cooling. *Earth Planet. Sci. Lett.* 241, 248–259.
- Egli, R., 2004. Characterization of individual rock magnetic components by analysis of remanence curves, 1. Unmixing natural sediments. *Stud. Geophys. Geod.* 48, 391–446.
- Egli, R., Chen, A.P., Winklhofer, M., Kodama, K.P., Horng, C.-S., 2010. Detection of noninteracting single domain particles using first-order reversal curve diagrams. *Geochim. Geophys. Geosyst.* 11, Q01Z11. <http://dx.doi.org/10.1029/2009GC002916>.
- Evans, M.E., Heller, F., 2001. Magnetism of loess/paleosol sequences: recent developments. *Earth-Sci. Rev.* 54, 129–144.
- Evans, M.E., Heller, F., 2003. *Environmental Magnetism*. Elsevier, New York.
- Fang, X.M., 1994. The origin and provenance of Malan loess from the eastern edge of Tibetan Plateau and its adjacent areas. *Sci. China Ser. B* 24, 539–546.
- Fang, X.M., Chen, F., Shi, Y., Li, J., 1996. Ganzhi Loess and the evolution of the cryosphere on the Tibetan Plateau. *Chin. Sci. Bull.* 41, 1865–1867.
- Ferrat, M., Weiss, D.J., Strelkopytov, S., Dong, S.F., Chen, H.Y., Najorka, J., Sun, Y.B., Gupta, S., Tada, R., Sinha, R., 2011. Improved provenance tracing of Asian dust sources using rare earth elements and selected trace elements for paleomonsoon studies on the eastern Tibetan Plateau. *Geochim. Cosmochim. Acta* 75, 6374–6399.
- Fontes, M.P.F., Weed, S.B., 1991. Iron oxides in selected Brazilian oxisols: I. Mineralogy. *Soil Sci. Soc. Am. J.* 55, 1143–1149.
- Forster, T., Heller, F., Evans, M.E., Havlíček, P., 1996. Loess in the Czech Republic: magnetic properties and paleoclimate. *Stud. Geophys. Geod.* 40, 243–261.
- Gallet, S., Jahn, B.M., Torii, M., 1996. Geochemical characterization of the Luochuan loess–paleosol sequence, China, and paleoclimatic implications. *Chem. Geol.* 133, 67–88.
- Geiss, C.E., Zanner, C.W., 2006. How abundant is pedogenic magnetite? Abundance and grain size estimates for loessic soils based on rock magnetic analyses. *J. Geophys. Res.* 111, B12521. <http://dx.doi.org/10.1029/2006jb004564>.
- Geiss, C.E., Zanner, C.W., 2007. Sediment magnetic signature of climate in modern loessic soils from the Great Plains. *Quat. Int.* 162–163, 97–110.
- Guo, B., Zhu, R.X., Roberts, A.P., Florindo, F., 2001. Lack of correlation between paleoprecipitation and magnetic susceptibility of Chinese loess/paleosol sequences. *Geophys. Res. Lett.* 28, 4259–4262.
- Hajdú, A., Illés, E., Tombácz, E., Borbáth, I., 2009. Surface charging, polyanionic coating and colloid stability of magnetite nanoparticles. *Colloids Surf. A, Physicochem. Eng. Asp.* 347, 104–108.
- Heller, F., Shen, C.D., Beer, J., Liu, X.M., Liu, T.S., Bronger, A., Suter, M., Bonani, G., 1993. Quantitative estimates of pedogenic ferromagnetic mineral formation in Chinese loess and paleoclimatic implications. *Earth Planet. Sci. Lett.* 114, 385–390.
- Heslop, D., Roberts, A.P., 2012a. A method for unmixing magnetic hysteresis loops. *J. Geophys. Res.* 117, B03103. <http://dx.doi.org/10.1029/2012gc004115>.
- Heslop, D., Roberts, A.P., 2012b. Estimation of significance levels and confidence intervals for first-order reversal curve distributions. *Geochim. Geophys. Geosyst.* 13, Q12240. <http://dx.doi.org/10.1029/2011jb008859>.
- Heslop, D., Roberts, A.P., 2013. Calculating uncertainties on predictions of palaeoprecipitation from the magnetic properties of soils. *Glob. Planet. Change* 110, 379–385.
- Heslop, D., Dekkers, M.J., Kruiver, P.P., van Oorschot, I.H.M., 2002. Analysis of isothermal remanent magnetization acquisition curves using the expectation-maximization algorithm. *Geophys. J. Int.* 148, 58–64.
- Hu, P.X., Liu, Q.S., Torrent, J., Barrón, V., Jin, C., 2013. Characterizing and quantifying iron oxides in Chinese loess/paleosols: implications for pedogenesis. *Earth Planet. Sci. Lett.* 369–370, 271–283.
- Hunt, C.P., Singer, M.J., Kletetschka, G., Tenpas, J., Verosub, K.L., 1995. Effect of citrate bicarbonate dithionite treatment on fine-grained magnetite and maghemite. *Earth Planet. Sci. Lett.* 130, 87–94.
- Ji, J.F., Chen, J., Balsam, W., Lu, H.Y., Sun, Y.B., Xu, H.F., 2004. High resolution hematite/goethite records from Chinese loess sequences for the last glacial–interglacial cycle: rapid climatic response of the East Asian Monsoon to the tropical Pacific. *Geophys. Res. Lett.* 31, L03207. <http://dx.doi.org/10.1029/2003gl018975>.
- Lai, Z.P., 2010. Chronology and the upper dating limit for loess samples from Luochuan section in the Chinese Loess Plateau using quartz OSL SAR protocol. *J. Asian Earth Sci.* 37, 176–185.
- Liu, J.F., Chen, J., Yin, J.H., Lu, Y.C., Murray, A., Chen, L.C., Thompson, J., Yang, H.L., 2010. OSL and AMS<sup>14</sup>C dating of the penultimate earthquake at the Leigu Trench along the Beichuan Fault, Longmen Shan, in the northeast margin of the Tibetan Plateau. *Bull. Seismol. Soc. Am.* 100, 2681–2688.
- Liu, Q.S., 2004. Pedogenesis and its effects on the natural remanent magnetization acquisition history of the Chinese loess. University of Minnesota, Minneapolis. PhD thesis.
- Liu, Q.S., Banerjee, S.K., Jackson, M.J., Maher, B.A., Pan, Y.X., Zhu, R.X., Deng, C.L., Chen, F.H., 2004a. Grain sizes of susceptibility and anhysteretic remanent magnetization carriers in Chinese loess/paleosol sequences. *J. Geophys. Res.* 109, B03101. <http://dx.doi.org/10.1029/2003jb002747>.
- Liu, Q.S., Jackson, M.J., Yu, Y.J., Chen, F.H., Deng, C.L., Zhu, R.X., 2004b. Grain size distribution of pedogenic magnetic particles in Chinese loess/paleosols. *Geophys. Res. Lett.* 31, L22603. <http://dx.doi.org/10.1029/2004GL021090>.
- Liu, Q.S., Torrent, J., Maher, B.A., Yu, Y.J., Deng, C.L., Zhu, R.X., Zhao, X., 2005. Quantifying grain size distribution of pedogenic magnetic particles in Chinese loess and its significance for pedogenesis. *J. Geophys. Res.* 110, B11102. <http://dx.doi.org/10.1029/2005JB003726>.
- Liu, Q.S., Deng, C.L., Torrent, J., Zhu, R.X., 2007. Review of recent developments in mineral magnetism of the Chinese loess. *Quat. Sci. Rev.* 26, 368–385.
- Liu, Q., Barrón, V., Torrent, J., Eeckhout, S.G., Deng, C., 2008. Magnetism of intermediate hydromaghemite in the transformation of 2-line ferrihydrite into hematite and its paleoenvironmental implications. *J. Geophys. Res.* 113, B01103. <http://dx.doi.org/10.1029/2007jb005207>.
- Liu, Q.S., Torrent, J., Morrás, H., Hong, A., Jiang, Z.X., Su, Y.L., 2010. Superparamagnetism of two modern soils from the northeastern Pampean region, Argentina and its paleoclimatic indications. *Geophys. J. Int.* 183, 695–705.
- Liu, Q.S., Roberts, A.P., Larrasoána, J.C., Banerjee, S.K., Guyodo, Y., Tauxe, L., Oldfield, F., 2012. Environmental magnetism: principles and applications. *Rev. Geophys.* 50, RG4002. <http://dx.doi.org/10.1029/2012rg000393>.
- Liu, Y., Shi, Z.T., Deng, C.L., Su, H., Zhang, W.X., 2012. Mineral magnetic investigation of the Taledo loess–paleosol sequence since the last interglacial in the Yili Basin in the Asian interior. *Geophys. J. Int.* 190, 267–277.
- Liu, Z.F., Colin, C., Li, X.J., Zhao, Y.L., Tuo, S.T., Chen, Z., Siringan, F.P., Liu, J.T., Huang, C.Y., You, C.F., Huang, K.F., 2010. Clay mineral distribution in surface sediments of the northeastern South China Sea and surrounding fluvial drainage basins: source and transport. *Mar. Geol.* 277, 48–60.
- Liu, Z.F., Liu, Q.S., Torrent, J., Barrón, V., Hu, P.X., 2013. Testing the magnetic proxy  $\chi_{FD}/\text{HRM}$  for quantifying paleoprecipitation in modern soil profiles from Shaanxi Province, China. *Glob. Planet. Change* 110, 368–378.
- Liu, Z.F., Liu, Q.S., 2014. Magnetic properties of two soil profiles from Yan'an, Shaanxi Province and their implications for paleorainfall reconstruction. *Sci. China Earth Sci.* 57, 1–10.
- Maher, B.A., 1988. Magnetic-properties of some synthetic sub-micron magnetites. *Geophys. J.* 94, 83–96.
- Maher, B.A., 1998. Magnetic properties of modern soils and Quaternary loessic paleosols: paleoclimatic implications. *Palaeogeogr. Palaeoclimatol. Palaeoecol.* 137, 25–54.
- Maher, B.A., Thompson, R., 1991. Mineral magnetic record of the Chinese loess and paleosols. *Geology* 19, 3–6.
- Maher, B.A., Thompson, R., 1995. Paleorainfall reconstructions from pedogenic magnetic susceptibility variations in the Chinese loess and paleosols. *Quat. Res.* 44, 383–391.
- Maher, B.A., Thompson, R., Zhou, L.P., 1994. Spatial and temporal reconstructions of changes in the Asian monsoon: a new mineral magnetic approach. *Earth Planet. Sci. Lett.* 125, 461–471.
- Mehra, O.P., Jackson, M.J., 1960. Iron oxide removal from soils and clays by a dithionite–citrate system buffered with sodium bicarbonate. *Clays Clay Miner.* 7, 317–327.
- Michel, F.M., Barrón, V., Torrent, J., Morales, M.P., Serna, C.J., Boily, J.F., Liu, Q.S., Ambrosini, A., Ciasmasu, A.C., Brown, G.E., 2010. Ordered ferrimagnetic form of

- ferrihydrite reveals links among structure, composition, and magnetism. *Proc. Natl. Acad. Sci. USA* 107, 2787–2792.
- Muxworthy, A.R., Dunlop, D.J., 2002. First-order reversal curve (FORC) diagrams for pseudo-single-domain magnetites at high temperature. *Earth Planet. Sci. Lett.* 203, 369–382.
- Nawrocki, J., Wojcik, A., Bogucki, A., 1996. The magnetic susceptibility record in the Polish and western Ukrainian loess–paleosol sequences conditioned by paleoclimate. *Boreas* 25, 161–169.
- Oldfield, F., 1991. Environmental magnetism — a personal perspective. *Quat. Sci. Rev.* 10, 73–85.
- Orgeira, M., Egli, R., Compagnucci, R., 2011. A quantitative model of magnetic enhancement in loessic soils. In: Petrovský, E., Ivers, D., Harinarayana, T., Herrero-Bervera, E. (Eds.), *The Earth's Magnetic Interior*. Springer, Netherlands, pp. 361–397.
- Pan, B., Wang, J., 1999. Loess record of Qinghai-Xizang Plateau monsoon variations in the eastern part of the plateau since the last interglacial. *Quat. Sci.* 4, 330–335 (in Chinese).
- Pike, C.R., Roberts, A.P., Verosub, K.L., 1999. Characterizing interactions in fine magnetic particle systems using first order reversal curves. *J. Appl. Phys.* 85, 6660–6667.
- Pike, C.R., Roberts, A.P., Verosub, K.L., 2001. First-order reversal curve diagrams and thermal relaxation effects in magnetic particles. *Geophys. J. Int.* 145, 721–730.
- Porter, S.C., Hallet, B., Wu, X., An, Z., 2001. Dependence of near-surface magnetic susceptibility on dust accumulation rate and precipitation on the Chinese Loess Plateau. *Quat. Res.* 55, 271–283.
- Pye, K., 1995. The nature, origin and accumulation of loess. *Quat. Sci. Rev.* 14, 653–667.
- Qiao, Y.S., Zhao, Z., Wang, Y., Wang, S., Fu, J., Li, C.Z., Jiang, F., 2006. Magnetostratigraphy and its paleoclimatic significance of a loess–soil sequence from Ganzhi area, west Sichuan Plateau. *Quat. Sci.* 26, 250–256 (in Chinese).
- Roberts, A.P., Pike, C.R., Verosub, K.L., 2000. First-order reversal curve diagrams: a new tool for characterizing the magnetic properties of natural samples. *J. Geophys. Res.* 105, 28461–28475.
- Roberts, A.P., Liu, Q.S., Rowan, C.J., Chang, L., Carvallo, C., Torrent, J., Horng, C.S., 2006. Characterization of hematite ( $\alpha$ -Fe<sub>2</sub>O<sub>3</sub>), goethite ( $\alpha$ -FeOOH), greigite (Fe<sub>3</sub>S<sub>4</sub>), and pyrrhotite (Fe<sub>7</sub>S<sub>8</sub>) using first-order reversal curve diagrams. *J. Geophys. Res.* 111, B12S35. <http://dx.doi.org/10.1029/2006jb004715>.
- Schwertmann, U., Fechter, H., 1984. The influence of aluminum on iron oxides: XI. Aluminum-substituted maghemite in soils and its formation. *Soil Sci. Soc. Am. J.* 48, 1462–1463.
- Singer, M.J., Bowen, L.H., Verosub, K.L., Fine, P., Tenpas, J., 1995. Mossbauer spectroscopic evidence for citrate–bicarbonate–dithionite extraction of maghemite from soils. *Clays Clay Miner.* 43, 1–7.
- Sun, J., Li, S.-H., Muhs, D.R., Li, B., 2007. Loess sedimentation in Tibet: provenance, processes, and link with Quaternary glaciations. *Quat. Sci. Rev.* 26, 2265–2280.
- Sun, Y.B., Tada, R., Chen, J., Liu, Q.S., Toyoda, S., Tani, A., Ji, J., Isozaki, Y., 2008. Tracing the provenance of fine-grained dust deposited on the central Chinese Loess Plateau. *Geophys. Res. Lett.* 35, L01804. <http://dx.doi.org/10.1029/2007GL031672>.
- Taylor, S.R., McLennan, S.M., 1985. *The Continental Crust: Its Composition and Evolution*. Blackwell, Oxford.
- Thompson, R., Oldfield, F., 1986. *Environmental Magnetism*. Allen and Unwin, London.
- Torrent, J., Liu, Q.S., Bloemendal, J., Barrón, V., 2007. Magnetic enhancement and iron oxides in the upper Luochuan loess–paleosol sequence, Chinese Loess Plateau. *Soil Sci. Soc. Am. J.* 71, 1570–1578.
- Vayssières, L., Chanéac, C., Tronc, E., Jolivet, J.P., 1998. Size tailoring of magnetite particles formed by aqueous precipitation: an example of thermodynamic stability of nanometric oxide particles. *J. Colloid Interface Sci.* 205, 205–212.
- Verosub, K.L., Roberts, A.P., 1995. Environmental magnetism: past, present, and future. *J. Geophys. Res.* 100, 2175–2192.
- Wang, Y.S., Li, Y.Z., Xiang, F., 2003. The Ganzhi loess origin in the west Sichuan Plateau. *J. Geomech.* 9, 91–96.
- Wei, H.T., Banerjee, S.K., Xia, D.S., Jackson, M.J., Jia, J., Chen, F.H., 2013. Magnetic characteristics of loess–paleosol sequences on the north slope of the Tianshan Mountains, northwestern China and their paleoclimatic implications. *Chin. J. Geophys.* 56, 150–158 (in Chinese).
- Worm, H.U., 1998. On the superparamagnetic-stable single domain transition for magnetite, and frequency dependence of susceptibility. *Geophys. J. Int.* 133, 201–206.
- Worm, H.U., Jackson, M., Banerjee, S.K., Schlinger, C.M., 1991. Magnetic viscosity of single domain magnetite particles. *J. Appl. Phys.* 59, 5533–5537.
- Yang, S., Fang, X., Shi, Z., Lehmkuhl, F., Song, C., Han, Y., Han, W., 2010. Timing and provenance of loess in the Sichuan Basin, southwestern China. *Palaeogeogr. Palaeoclimatol. Palaeoecol.* 292, 144–154.
- Yang, T.S., Hyodo, M., Zhang, S.H., Maeda, M., Yang, Z.Y., Wu, H.C., Li, H.Y., 2013. New insights into magnetic enhancement mechanism in Chinese paleosols. *Palaeogeogr. Palaeoclimatol. Palaeoecol.* 369, 493–500.
- Zan, J., Fang, X., Yang, S., Nie, J., Li, X., 2010. A rock magnetic study of loess from the West Kunlun Mountains. *J. Geophys. Res.* 115, B10101. <http://dx.doi.org/10.1029/2009JB007184>.
- Zhang, Q.G., Kang, S.C., Kaspari, S., Li, C.L., Qin, D.H., Mayewski, P.A., Hou, S.G., 2009. Rare earth elements in an ice core from Mt. Everest: seasonal variations and potential sources. *Atmos. Res.* 94, 300–312.
- Zhang, W.G., Yu, L.Z., Lu, M., Zheng, X.M., Shi, Y.X., 2007. Magnetic properties and geochemistry of the Xiashu loess in the present subtropical area of China, and their implications for pedogenic intensity. *Earth Planet. Sci. Lett.* 260, 86–97.
- Zhou, L.P., Oldfield, F., Wintle, A.G., Robinson, S.G., Wang, J.T., 1990. Partly pedogenic origin of magnetic variations in Chinese Loess. *Nature* 346, 737–739.